Structural Symmetry: The Three-Dimensional Structure of *Haemophilus Influenzae* Diaminopimelate Epimerase[†,‡]

Maurizio Cirilli,[§,||] Renjian Zheng,[§] Giovanna Scapin,*[,⊥] and John S. Blanchard*[,§]

Department of Biochemistry, Albert Einstein College of Medicine, 1300 Morris Park Avenue, Bronx, New York 10461, Instituto di Strutturistica Chimica, CNR, Area della Ricerca di Roma, Monterotondo, Roma, Italy, and Merck Research Laboratories, RY50-105, P.O. Box 2000, Rahway, New Jersey 07065

Received September 3, 1998; Revised Manuscript Received October 9, 1998

ABSTRACT: The *Haemophilus influenzae* diaminopimelate epimerase was cloned, expressed, purified, and crystallized in the $C222_1$ space group ($a = 102.1$ Å, $b = 115.4$ Å, $c = 66.3$ Å, $\alpha = \beta = \gamma = 90°$). The three-dimensional structure was solved to 2.7 Å using a single Pt derivative and the Se-Met-substituted enzyme to a conventional *R* factor of 19.0% ($R_{free} = 24.2\%$). The 274 amino acid enzyme consists of two structurally homologous domains, each containing eight β-strands and two α-helices. Diaminopimelate epimerase is a representative of the PLP-independent amino acid racemases, for which no structure has yet been determined and substantial evidence exists supporting the role of two cysteine residues as the catalytic acid and base. Cys73 of the amino terminal domain is found in disulfide linkage, at the domain interface, with Cys217 of the carboxy terminal domain, and we suggest that these two cysteine residues in the reduced, active enzyme function as the acid and base in the mechanism.

The epimerization of L,L- to D,L-*meso*-diaminopimelate (DAP) was first demonstrated by Work (*1*) in extracts of *Aerobacter aerogenes*, and the enzyme catalyzing this reaction, diaminopimelate epimerase (EC 5.1.1.7, Figure 1, top) was subsequently purified and characterized from *Escherichia coli* (*2*). The biosynthesis of *meso*-D,L-DAP, the immediate precursor of L-lysine in bacteria, is a multistep process beginning with the phosphorylation and reduction of L-aspartate to yield L-aspartate semialdehyde (Figure 1, bottom). This molecule is subsequently condensed with pyruvate, to yield the complete seven carbon diaminopimelate skeleton, and reduced to yield tetrahydrodipicolinate. This compound can be directly converted to *meso*-DAP by DAP dehydrogenase (*3*) or via parallel pathways involving α-L-amino acid succinylation or acetylation, depending on the bacterial genera. Either of these latter two pathways yield L,L-DAP, which must be converted to D,L-DAP by the epimerase prior to decarboxylation to generate L-lysine.

The *dapF* gene, encoding DAP epimerase, was cloned and mapped in *E. coli* (*4*), and its sequence was reported the following year (*5*). The recombinant *E. coli* epimerase has been expressed and shown to be stoichiometrically inactivated by an active-site-directed aziridine derivative of diaminopimelate [aziDAP, 2-(4-amino-4-carboxybutyl)aziri-

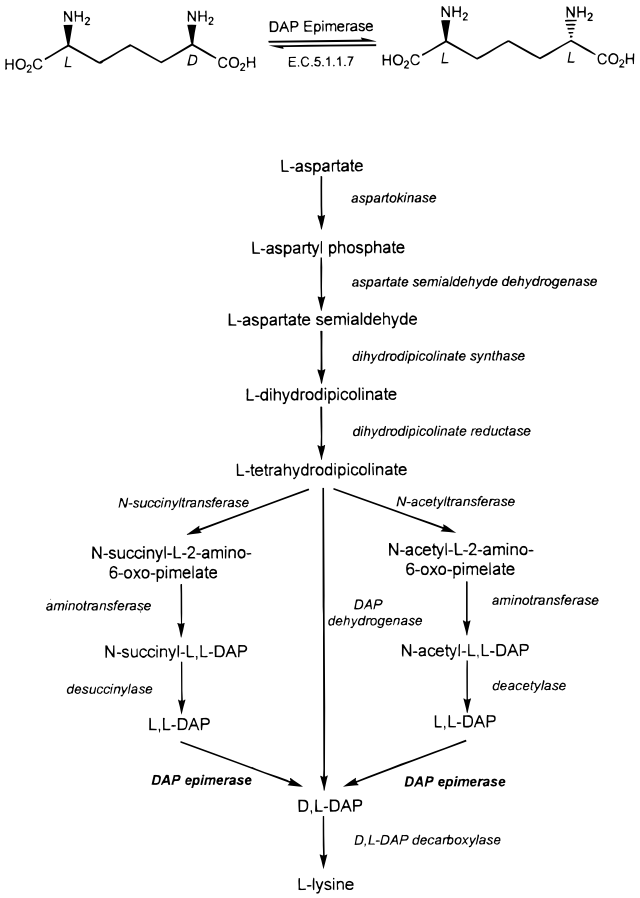

FIGURE 1: (Top) Reaction catalyzed by Diaminopimelate Epimerase. (Bottom) The bacterial biosynthetic pathway for L-lysine. The *dapF*-encoded DAP epimerase represents the eighth step in the pathway.

[†] This work was supported by the National Institutes of Health (AI33696) and Merck Research Laboratories.

[‡] The coordinates of Diaminopimelate Epimerase have been deposited in the Brookhaven Protein Data Bank (filename 1BWZ).

* To whom correspondence should be addressed. (G.S) E-mail: giovanna_scapin@merck.com. (J.S.B.) E-mail: blanchar@aecom.yu.edu. Phone: 718-430-3096. Fax: 718-430-8565.

[§] Albert Einstein College of Medicine.

[||] CNR.

[⊥] Merck Research Laboratories.

10.1021/bi982138o CCC: $15.00
Published on Web 11/04/1998

dine-2-carboxylate (*6*, *7*)]. The irreversible inhibition of the epimerase by aziDAP is due to the alkylation of Cys73, suggesting that this residue is present at or near the active site (*6*).

The racemization of amino acids is important to provide substrates for the construction of bacterial peptidoglycan, which contains a number of D-amino acid centers. Thus, alanine racemase (EC 5.1.1.1) catalyzes the PLP-dependent conversion of L- to D-alanine, which is then incorporated into the D-alanine-D-alanine terminus of the pentapeptide precursor to the mature cross-linked peptidoglycan. This enzyme has been thoroughly mechanistically studied, and the three-dimensional structure of the *Bacillus stearothermophilus* enzyme has recently been determined and shown to be a member of the $(\alpha/\beta)_8$ structural family (*8*). The PLP-independent amino acid racemases have been the subject to similar mechanistic scrutiny. The reactions catalyzed by proline racemase (*9*, *10*) and glutamate racemase (*11*, *12*) are notable in this regard, since both appear to operate by "two-base" mechanisms and utilize a thiolate as the general base and a thiol as the general acid. The lack of PLP, and the potential involvement of cysteine as an active-site residue, has led to the comparison of the reaction of diaminopimelate epimerase to the reactions catalyzed by proline and glutamate racemases. While these two enzymes bear substantial mechanistic similarity, the active-site thiols in proline racemase appear to be contributed by separate subunits of the 38 kDa dimer (*9*), whereas the active-site thiols in glutamate racemase appear to be contributed by Cys73 and Cys184 of the same subunit of the 28.3 kDa monomeric enzyme (*11*).

We report here the expression, purification, crystallization, and determination of the three-dimensional structure of the *Haemophilus influenzae* diaminopimelate epimerase to 2.7 Å. The 274 amino acid enzyme exhibits a novel fold, in which the amino terminal and carboxyl terminal halves of the molecule fold into structurally homologous domains. The residue which is alkylated by aziDAP and Cys73 is at the interface of the two domains and is in disulfide linkage with Cys217. We suggest that these two residues, upon reduction, are the general acid and general base responsible for reversible Cα−H bond cleavage by diaminopimelate epimerase.

MATERIALS AND METHODS

Cloning, Expression, and Purification. The *dapF* gene encoding DAP epimerase was obtained by PCR amplification of the gene from genomic DNA of *H. influenzae* RD (ATCC), using Pfu DNA polymerase and two primers (5′-TACATATGCAGTTTTCCAAAATGCAC-3′; 5′-CGGGATCCGTTAAAGAGTTATAAACCCATCATA-3′) containing *Nde*I and *Bam*HI restriction sites, respectively. The *dapF* gene was inserted into an *Nde*I- and *Bam*HI-digested pET 23a(+) plasmid. The recombinant plasmid was transferred into the competent *E. coli* strain BL21(DE3). The BL21-(DE3) transformants containing pET 23a(+)-*dapF* were grown at 37 °C to an A_{600} of 0.5 in LB medium containing 50 μg/mL carbenicillin. IPTG was added to the culture (final [IPTG] = 0.5 mM), and growth was continued for an additional 3 h at 37 °C. The SeMet-substituted DAP epimerase was prepared using the methionine auxotroph B834 (DE3) *E. coli* strain (Novagen). After transformation with pET23a(+)-*dapF*, the transformed B834(DE3) cells were grown in M9 medium containing 50 μg/mL carbenicillin and supplemented with selenomethionine. The cells were grown at 37 °C for 12 h to an A_{600} of 0.3, induced by the addition of IPTG (final [IPTG] = 0.5 mM), and grown for an additional 12 h.

All purification steps were performed at 4 °C. Cells (6 g) were suspended in 30 mL of 40 mM triethanolamine-HCl, pH 7.8, containing 100 μM DTT, 1 mM EDTA, protease inhibitors (Boehringer Mannheim), and 6 mg of lysozyme and stirred for 30 min at 4 °C. The cells were disrupted by sonication, and cell debris was removed by centrifugation for 45 min at 11 000 rpm. Nucleic acids were precipitated by the addition of streptomycin sulfate (1% w/v final) to the supernatant, and the nucleic acids were pelleted by centrifugation for 45 min at 11 000 rpm. The supernatant was dialyzed against 20 mM triethanolamine-HCl, pH 7.8, containing 100 μM DTT and 1 mM EDTA. The precipitate which formed during dialysis was removed by ultracentrifugation. The supernatant was applied to a 140 mL Fast Flow Q-Sepharose anion-exchange column, and proteins were eluted with a linear 0 to 0.8 M NaCl gradient. Active fractions were pooled, and protein was precipitated by the addition of ammonium sulfate to 30% saturation. The 30% $(NH_4)_2SO_4$ pellet was collected by centrifugation and dissolved in, and dialyzed against, 20 mM triethanolamine-HCl, pH 7.8, containing 100 μM DTT, 1 mM EDTA, and 0.5 M ammonium sulfate. After centrifugation to remove insoluble material, the supernatant was applied to a Phenyl Sepharose column and proteins were eluted with a linear 0.5 to 0 M $(NH_4)_2SO_4$ gradient. The active fractions, which were homogeneous as evidenced by a single band on SDS−PAGE, were pooled. Electrospray ionization/mass spectrometry was performed on both WT and SeMet forms of DAP epimerase and confirmed that no mutations were introduced during PCR and to confirm the degree of substitution of SeMet in the enzyme.

Crystallization. Crystals of *H. influenzae* DAP epimerase were grown using the hanging drop vapor diffusion technique at constant temperature (15 °C). Typically, 3 μL of a protein solution (20 mg/mL in 25 mM HEPES, pH 7.5, containing 0.05% NaN_3) was added to 3 μL of the reservoir solution (1 M sodium acetate in 0.1 M sodium cacodylate, pH 6.8). Crystals appeared after 2 days and reached their maximum dimensions (0.2 mm × 0.4 mm × 0.7 mm) within 5 days. The crystals were tetrahedral in shape and belong to the orthorhombic $C222_1$ space group with unit cell dimensions of $a = 102.1$ Å, $b = 115.4$ Å, $c = 66.3$ Å. There was one molecule in the asymmetric unit, corresponding to a solvent content of about 62%. Crystals of the selenomethionine-substituted enzyme were grown under the same conditions, but took about 4 days to appear and about 9 days to reach their maximum dimensions.

Data Collection and Heavy Atom Screening. All diffraction data were collected at constant temperature (15 °C) on a Siemens multiwire area detector using a Rigaku rotating anode operating at 50 kV and 80 mA as the X-ray source. Each frame covered 0.25 °C and was measured for 90 s for the native and 180−200 s for the derivative datasets. Intensity data were reduced and converted to structure factors by the XENGEN system software (*13*) running on a Silicon

Table 1: Summary of Crystallographic Data

space group	$C222_1$
unit cell parameters	
a (Å)	102.1
b (Å)	115.4
c (Å)	66.3
$\alpha = \beta = \gamma$ (deg)	90

Diffraction Data Statistics

	native	K_2PtCl_4	SeMet
resolution (Å)	2.7	2.5	2.7
total observations	33 313	26 520	43 919
unique reflections	7946	11 756	10 144
completeness (%), all data (last shell)	89.4 (51.6)	83.0 (66.0)	88.3 (50.6)
R_{sym}[a] (%) (last shell)	6.0 (14.5)	7.2 (18.7)	8.8 (20.9)
$\langle I/\sigma(I)\rangle$ (last shell)	12.6 (6.2)	9.2 (3.3)	10.3 (5.7)
R_{iso}[b] (%)		10.5	9.0

Phasing Statistics

resolution (Å)					23.0−3.0		23.0−3.0	
no. of sites					2		7	
phasing power[c] (centric/acentric)					1.18/1.36		1.13/1.38	
R_{Cullis}[d] (Å)					0.771		0.781	
R_{Kraut}[e] (Å)					0.178		0.141	
resolution (Å)	7.6	5.4	4.5	3.9	3.5	3.2	3.0	overall
no. of reflections	504	809	1010	1200	1276	1325	1088	7212
mean figure of merit	.616	.508	.396	.305	.237	.179		0.354

Refinement Statistics

resolution (Å)	2.7
non-hydrogen atoms	2117
water molecules	29
R_{factor}[f]	0.190
R_{free}[g]	0.242
rms deviation for bond lengths (Å)	0.004
rms deviation for angles (deg)	0.825
rms deviation for dihedral angles (deg)	28.59
avg B factors (Å^2)	
protein	37.7
waters	41.3

[a] $R_{sym} = \sum|I - \langle I\rangle|/\sum\langle I\rangle$ where I is the observed intensity and $\langle I\rangle$ is the average intensity of multiple observations of symmetry-related reflections. [b] $R_{iso} = \sum|F_{PH} - F_P|/\sum F_P$, where F_{PH} and F_P are the observed derivative and native structure factor amplitudes. [c] Phasing power $= \sum|F_{H(calc)}|/\sum|E_c|$, where F_H is the structure factor of the heavy atoms and E_c (=lack of closure) $= |F_{PH(obs)} - F_{PH(calc)}|$. [d] $R_{cullis} = \langle E_c\rangle/\langle\Delta_c\rangle$, where E_c is the lack of closure for centric reflections and Δ_c is the isomorphous difference for centric reflections. [e] $R_{kraut} = \langle E_c\rangle/F_{PH(obs)}$. [f] $R_{factor} = \sum|F_P - F_{P(calc)}|/\sum F_P$. [g] R_{free} is the R_{factor} calculated for a subset of 7% of the reflection data that were not included in the refinement.

Graphics computer. To obtain heavy atom derivatives, crystals were soaked in over 50 solutions of heavy atom compounds using different concentrations and soaking times, and diffraction data were collected and reduced as described above. Generally, 24 h soaks of crystals in the reservoir solution containing 1 mM heavy atom were the starting conditions for this search, although shorter soaking times and lower concentrations of heavy metal were extensively tested. A single Pt derivative was obtained by soaking crystals for 3 h in a mother liquor-like solution containing 2 mM of K_2PtCl_4. A summary of the statistics for data collection of native, Pt derivative, and Se-Met-substituted enzymes is shown in Table 1.

Structure Solution, Model Building, and Refinement. The structure was determined at 2.7 Å resolution by the Multiple Isomorphous Replacement (MIR) method using the Pt and SeMet datasets as phase sources. All the phasing steps were carried out using the program SHARP (*14*). Two heavy atom positions for the Pt derivative were identified from difference Patterson maps against the native data calculated with PHASES (*15*). Seven of the nine Se atom positions in the SeMet protein were identified by the cross difference Fourier technique using the phases calculated from the Pt derivative. The heavy atom coordinates were refined and the corresponding phases calculated to 3.0 Å. The MIR phases obtained (overall FOM = 0.354) were subjected to 130 cycles of solvent flattening procedures, and extended to 2.7 Å using SOLOMON (*16*). The resulting skeletonized solvent-flattened MIR map permitted a clear interpretation of the secondary structure elements and of many of the side chains.

The program O (*17*) was used to build a partial Cα backbone, and a polyalanine molecule was subsequently built to include 93% of the total residues. The positions of the seven Se atoms, refined in the phasing step, were used as a guide to register the placement of the amino acid side chains into the electron density map. Model refinement was carried out by simulating annealing and B-refinement procedures as implemented in X-PLOR (*18*). Before refinement, a randomly selected 7% of the data was flagged to make them unavailable for subsequent refinement and used as "test set" for statistical cross-validation purposes (*19*). Initial refinement of the polyalanine model was carried out by simulating annealing-torsional dynamics (*20*) using 15.0−2.7 Å data

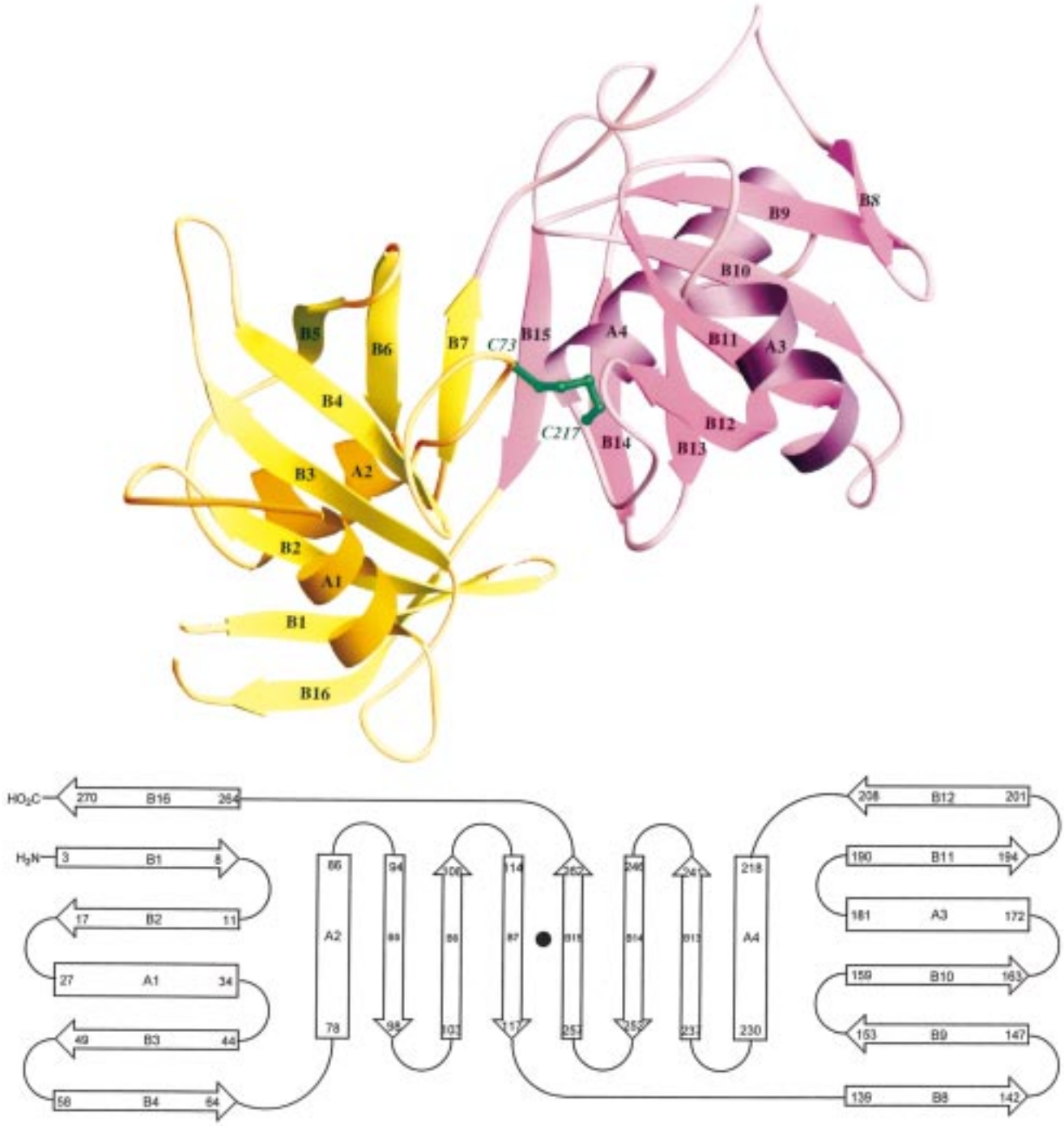

FIGURE 2: (A, top) Ribbon Diagram on *H. influenzae* DAP epimerase. The N- and C-termini are labeled, as are the secondary structural elements and the two conserved cysteines. Domain I (residues 1−117 and 263−274) is shown in yellow, Domain II (residues 118−262) is shown in magenta and the disulfide connecting the two domains is shown in green. This figure, as well as Figures 3 and 5, were generated using RIBBONS (27). (B, bottom) Topology of the secondary structural elements of *H. influenzae* DAP epimerase. The position of the pseudo-2-fold symmetry axis relating the two domains is indicated by the black dot between β-strands B7 and B8.

(previously bulk solvent corrected) in order to get a more favorable reflections/parameters ratio and a larger degree of convergence. In this step, the standard *R* factor dropped from ca. 42% to ca. 32% and the R_{free} from ca. 45% to ca. 41%. Several iterative cycles of simulating annealing procedures and manual rebuilding using Sigma-weighted (*21*) $2F_o - F_c$ and $F_o - F_c$ difference maps allowed us to trace the entire polypeptide chain and incorporate the amino acid sequence. Refinement was completed by individual B-refinement procedures. At this stage, water molecules were placed into positions that showed both the presence of residual 3σ $F_o - F_c$ peaks and $2F_o - F_c$ density and made stereochemically feasible hydrogen bonds to protein atoms. The final model contains 274 amino acid residues, with all but the last two (residues 273 and 274) side chains assigned, and 29 solvent molecules. Of the 274 residues, 85.9% is in the most favored region of the Ramachandran plot, 13.7% in the additionally allowed, and only 0.4% in the generously allowed regions, as defined in PROCHECK (*22*). The refinement statistics are summarized in Table 1.

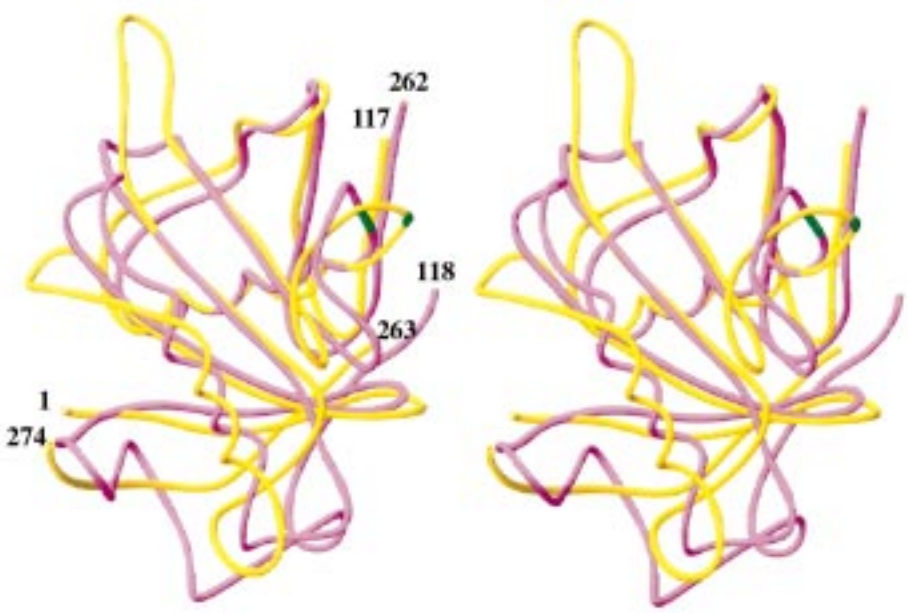

FIGURE 3: Stereoview of the superposition of domain I and II, which are colored in yellow and magenta, respectively. The rotation matrix relating the two subunits was calculated with O[17], and gave a rms fit of 1.78 Å for 99 Cα atoms.

RESULTS AND DISCUSSION

Description of the Structure. The *H. influenzae dapF*-encoded diaminopimelate epimerase is a monomeric, two-domain enzyme of 274 amino acids of overall cylindrical shape that measures approximately 53 × 23 × 25 Å. Figure 2A is a ribbon depiction of the enzyme, and Figure 2B is a topological representation of the secondary structural elements which make up the overall fold. The enzyme contains 16 β-strands (B1−B16 in Figure 2) and four α-helices (A1−A4). Each of the two domains, shown in magenta and yellow in all figures, contains eight β-strands and two α-helices, and the symmetry of the two domains is very evident. The individual domains can be superimposed with a root-mean-square deviation between equivalent Cα atoms of less than 2 Å (see below). The first domain is formed by the first 117 (Met1−Asn117) and the last 11 residues (Glu263−Leu274) of the polypeptide. β-Strand B1 (Phe3−Gly8) is antiparallel to B2 (Asn11−Asp17) and is connected to it by a short two residue loop. B2 and B3 (Gln44−Glu49) are parallel and are connected in a right-handed fashion by a crossover connection containing helix A1 (Pro27−Ala34). β-Strand 4 (B4, Phe58−Asn64) runs antiparallel to B3, and together with B16 (Thr265−Gly270), they make up a highly twisted five-stranded β-sheet (B4 and B16 are at a 78° angle). B4 is connected to B5 by helix A2 (Arg78−Leu86), which lies at an angle of about 70° across the amino terminal β-sheet. B5 (Asp94−Ser98) runs parallel to B4, but is shifted with respect to B4 such that only the three carboxy terminal residues of B4 and the three amino terminal residues of B5 are hydrogen bonded. Strands B5, B6 (Asn 103−Val108), and B7 (Ile114−Asn117) are antiparallel, with B5 and B6 connected by a type III β-turn (*23*) and with B6 and B7 connected by a five residue γ-turn (*24*). These three β-strands (B5−B7) form a second β-sheet that is almost perpendicular to the five-stranded β-sheet composed of B1−B4 and B16. This arrangement of eight β-strands is vaguely reminiscent of the β-clam motifs found in the fatty acid and retinol-binding proteins (*25*). Of the two helices in this domain, A1 is solvent exposed, while A2 is completely enclosed by the five-stranded and three-stranded β sheets.

The second domain is topologically almost identical to the first. The domain begins at the carboxy terminus of B7 and includes a long connecting loop (Met118−Asn138). β-Strands B8 (Tyr139−Arg142), B9 (Thr147−Val153), and B10 (His159−Gln163) are antiparallel, with B8 and B9 connected by a type III β-turn, and with B9 and B10 connected by a five residue loop. B10 is connected to B11 (Asn 190−Met194) by helix A3 (Val172−Ser181). B11 is connected to B12 (His201−Glu208) by a six residue turn, and B12 is the fifth of the β-strands which makes up the second five-stranded β-sheet. Helix A4 (Gly2180Met230) connects this β-sheet to the three-stranded β-sheet composed of the three antiparallel strands: B13 (Asn237−Asp241), B14 (Ser 246−Trp251), and B15 (Leu258−Gly262). B13 and B14 are connected by a type III β-turn, while B14 and B15 are connected by a six residue β-bulge loop (*24*). B15 runs antiparallel and is hydrogen bonded to B7, providing an interaction between the two three-stranded antiparallel sheets of the two domains. Helix A3, like A1, is solvent exposed, while helix A4, like A2, is enclosed on either side by the five-stranded and three-stranded β-sheets.

Structural Symmetry. The DAP epimerase structure represents a novel fold that does not have any homologue in the protein database [searched with DALI (*26*)]. The two domains that make up the monomer of diaminopimelate epimerase are structurally homologous, and are related by a pseudo-2-fold symmetry axis perpendicular to the B7 and B15 β-strands. Rotation around this axis juxtaposes domain II (residues 118−262, magenta) on top of domain I (residues 1−117 and 263−274, yellow) as shown in Figure 3. A rotation matrix calculated with O (*17*) using the secondary structure elements indicated in Figure 3 as probes demonstrates that the two domains can be overlaid with a root-mean-square deviation of equivalent α-carbon atoms of 1.78

Å for 99 residues out of 129 for domain I and 145 of domain II. This structural alignment was used to probe whether the amino acid sequences of the two domains could be aligned. Although there does not appear to be any significant primary sequence homology between the two domains (28.6% identity using primary sequence alone; 16.2% identity if secondary structural elements are aligned), the region of highest homology is centered around two cysteine residues, Cys73 and Cys217. The former residue has been previously identified as the residue which is alkylated by the active-site-directed irreversible aziridine inhibitor aziDAP. These two residues are present at the domain interface and are in two structurally homologous regions at the amino terminus of the α-helices (A2 and A4) connecting the five-stranded and three-stranded β-sheets. These residues are present in disulfide linkage, presumably due to their oxidation during crystallization (see below). Sequence similarity searches, using the *H. influenzae* amino acid sequence, revealed 12 additional potential DAP epimerases from various bacteria, but no other close homologues. Alignment of 13 bacterial *dapF*-encoded diaminopimelate epimerase reveals that, of the seven cysteines present in the *Haemophilus* epimerase, only Cys72 and 217 are conserved in these epimerase sequences from Gram-negative, Gram-positive, and archaebacterial species (Figure 4). A striking exception to the absolute conservation of Cys73 and Cys217 is found in the sequence of the *Anabena sp*. gene identified as a diaminopimelate epimerase, where the residues homologous to Cys73 and Cys217 are both serine residues.

The Cystine73−217 Disulfide. Like its mechanistically related non-PLP amino acid racemases, diaminopimelate requires the presence of a thiol reductant for maximal activity (*2*). Our earliest crystallization conditions included micromolar concentrations of DTT, but we failed to crystallize the enzyme under any conditions in which DTT was present. Crystallization was only observed in the absence of thiol reductant, and we clearly observe the presence of a normal left-handed disulfide between Cys73 and Cys217 connecting the two domains. The surface of the enzyme has a deep 20 Å long cleft separating the two domains (Figure 4, top). The Cys73−217 disulfide is positioned midway down this cleft, which is lined with polar and charged residues. A more detailed examination of the cleft region reveals a number of features relevant to catalysis (Figure 4, bottom). The loop containing Cys73 is highly mobile as evidenced by its higher temperature factor compared to the adjacent structural elements. The thiol of Cys73 is the residue that is alkylated by aziDAP (*6*), suggesting its higher relative nucleophilicity compared to Cys217. Also labeled in the figure are H159 and E208, residues that are completely conserved in all 13 bacterial Dap epimerase sequences. These two residues are located on opposite sides of the plane of the disulfide bond and may function to electrostatically interact with the α-carboxyl and α-amino groups of DAP, respectively. Alternatively, these residues may modulate the p*K* values of the two catalytic cysteine residues in the reduced enzyme. It is likely that, under the reducing conditions present intracellularly, the two domains are relatively free to move with respect to each other and that substrate binding occurs to an "open", more mobile form of the reduced enzyme. There are a limited number of interdomain interactions, primarily the hydrogen-bonding interactions between the

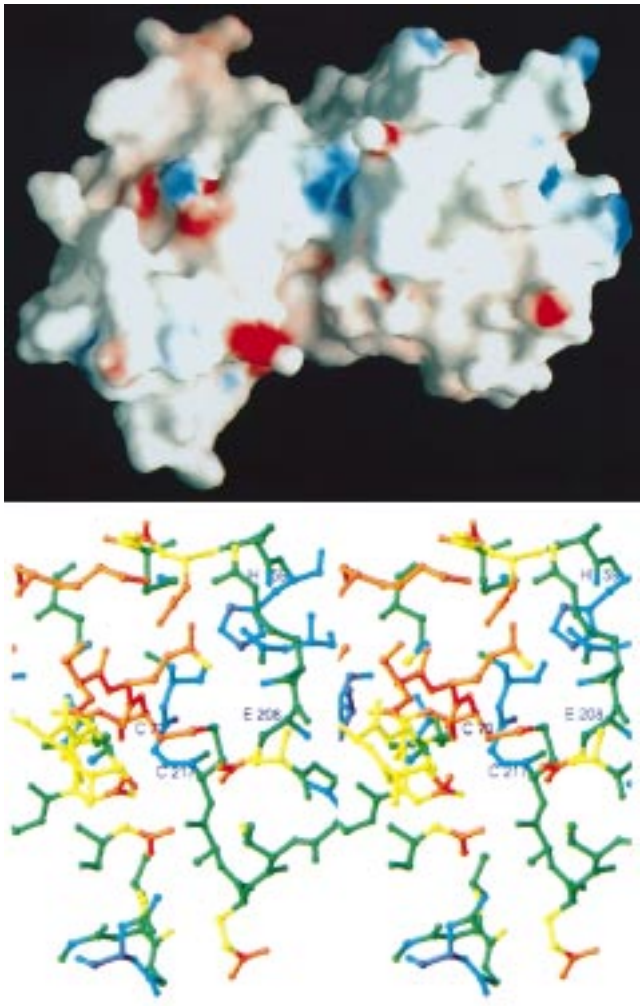

FIGURE 4: (Top) Surface of DAP Epimerase showing the cleft separating the two structurally homologous domains. The figure was made with GRASP (28) using the same orientation as that presented in Figure 2A. The electrostatic field contributed by individual cationic (blue) or anionic (red) residues is shown. (Bottom) Stereo, close-up view of the cleft region, including the C73-217 disulfide. Atoms are colored according to their temperature factors, with blue representing the lowest values of the *B* factors and red representing the highest values of the *B* factors.

antiparallel β-sheets, B7 and B15. The serendipitous formation of the Cys73−Cys217 disulfide bond may be critical to the stabilization of the enzyme in a rigid conformation, allowing for crystallization to occur.

We suggest a catalytic role for both Cys73 and Cys217 as the acid−base pair responsible for *pro*-R and *pro*-S proton abstraction. Substantial precedent for the presence of two "bases" at the active sites of both proline and glutamate racemase has been presented (*9*−*12*), including the loss of epimerase activity when either Cys73 or Cys184 of the *Lactobacillus fermenti* glutamate racemase are mutated into the corresponding alanine residues (*12*). The presence of two symmetrically disposed cysteine residues would appear to perfectly complement the formation of a symmetric transition state or carbanion intermediate. Finally, cysteine residues often function as nucleophiles in enzyme-catalyzed reactions, but rarely function as bases. The non-PLP amino acid racemases are a potentially unique enzymatic example where cysteine residues serve this function, and the structure of DAP epimerase reported here reveals how two such

residues may be positioned in a highly symmetric structure to perform the reversible, symmetric interconversion of enantiomeric amino acid centers. The structural determination of an enzyme−substrate or enzyme−inhibitor complex will be required to confirm this hypothesis.

REFERENCES

1. Antia, M., Hoare, D. S., and Work, E. (1957) *Biochem. J. 65*, 448−459.
2. Wiseman, J. S., and Nichols, J. S. (1984) *J. Biol. Chem. 259*, 8907−8914.
3. Scapin, G., Reddy, S. G., and Blanchard, J. S. (1997) *Biochemistry 35*, 13540−13551.
4. Richaud, C., Higgins, W., Mengin-Lecreulx, D., and Stragier, P. (1987) *J. Bacteriol. 169*, 1454−1459.
5. Richaud, C., and Printz, C. (1989) *Nucleic Acids Res. 16*, 10367.
6. Higgins, W., Tardif, C., Richaud, C., Krivanek, M. A., and Cardin, A. (1989) *Eur. J. Biochem. 186*, 137−145.
7. Gerhart, F., Higgins, W., Tardif, C., and Ducep, J.-B. (1990) *J. Med. Chem. 33*, 2157−2162.
8. Shaw, J. P., Petsko, G. A., and Ringe, D. (1997) *Biochemistry 36*, 1329−1342.
9. Rudnick, G., and Abeles, R. H. (1975) *Biochemistry 14*, 4515−4522.
10. Belasco, J. G., Albery, W. J., and Knowles, J. R. (1986) *Biochemistry 25*, 2552−2558.
11. Gallo, K. A., and Knowles, J. R. (1993) *Biochemistry* ***32***, 3981−3990.
12. Tanner, M. E., Gallo, K. A., and Knowles, J. R. (1993) *Biochemistry 32*, 3998−4006.
13. Howard, A. J. (1996) *A guide to data reduction for the Nicolet Imaging Proportional Counter: the XENGEN system*, Protein Engineering Department, GENEX corporation, 16020 Industrial Drive Gaithersburg, MD 20887.
14. De La Fortelle, E., and Bricogne, G. (1997) *Methods Enzymol. 276*, 472−494.
15. Furey, W., and Swaminathan, S. (1997) *Methods Enzymol. 277*, 590−620.
16. Abrahams, J. P., and Leslie, A. G. W. (1996) *Acta Crystallogr., Sect. D 52*, 30−42.
17. Jones, A. T., and Kjeldgaard, M. (1997) *Methods Enzymol.* ***277***, 173−208.
18. Brunger, A. T., Kuriyan, J., and Karplus, M. (1987) *Science* ***235***, 458−460; Brunger, A. T., Krukowski, J., and Erickson, J. (1990) *Acta Crystallogr., Sect. A 46*, 585−593.
19. Brunger, A. T. (1992) *Nature* ***355***, 472−474.
20. Rice, L. M., and Brunger, A. T. (1994) *Proteins: Struct., Funct., Genet. 19*, 277−290.
21. Read, R. J. (1986) *Acta Crystallogr., Sect. A 42*, 140−149.
22. Laskoswski, R. A., MacArthur, M. W., Moss, S. D., and Thornton, J. M. (1993) *J. Appl. Crystallogr. 26*, 283−291.
23. Richardson, J. S. (1981) *Adv. Protein Chem. 34*, 167−339.
24. Milner-White, E. J., and Poet, R. (1986) *Biochem. J. 240*, 289−292.
25. LaLonde J. M., Bernlohr D. A., and Banaszak, L. J. (1994) *FASEB J. 8*, 1240−1247.
26. Holm L and Sander C. (1993) *J. Mol. Biol. 233*, 123−138.
27. Carson, M. (1997) *Methods Enzymol. 277*, 493−505.
28. Nicholls, A., Sharp, K., and Honig, B. (1991) *Proteins: Struct., Funct., Genet. 11*, 281−296.

BI982138O